Sumargo Edwin (Orcid ID: 0000-0002-3671-7498)
McMillan Hilary (Orcid ID: 0000-0002-9330-9730)

Confidential manuscript submitted to Hydrological Processes

A Soil Moisture Monitoring Network to Assess Controls on Runoff Generation During Atmospheric River Events

Running Title: Soil Moisture Controls on Runoff Generation

Authors: Edwin Sumargo[1,*], Hilary McMillan[2], Rachel Weihs[1], Carolyn J. Ellis[1], Anna M. Wilson[1], and F. Martin Ralph[1]

Affiliations:

[1]*Center for Western Weather and Water Extremes, Scripps Institution of Oceanography (CW3E), University of California San Diego, La Jolla, CA, USA*

[2]*Department of Geography, San Diego State University, San Diego, CA, USA*

Acknowledgments

This study was largely carried out with aid from NOAA Hydrometeorology Testbed (Grant no. NA17OAR4590185). Support for the CW3E observational network is provided by Sonoma Water and the United States Army Corps of Engineers (Grant no. W912HZ-15-2-0019). The network is run and maintained by the CW3E of Scripps Institution of Oceanography. We thank Luca Delle Monache for his feedback, Brian Henn for the soil cluster analysis, Douglas Alden and Stephen Turnbull for their field technical assistance, and Patrick Mulrooney for his computational assistance.

[*]Corresponding author: Edwin Sumargo (esumargo@ucsd.edu)

Reference Addition

MacQueen, J. (1967, June). Some methods for classification and analysis of multivariate observations. In *Proceedings of the fifth Berkeley symposium on mathematical statistics and probability* (Vol. 1, No. 14, pp. 281-297).

A Soil Moisture Monitoring Network to Assess Controls on Runoff Generation During Atmospheric River Events

Abstract

Soil moisture is a key modifier of runoff generation from rainfall excess, including during extreme precipitation events associated with Atmospheric Rivers (ARs). This paper presents a new, publicly available dataset from a soil moisture monitoring network in Northern California's Russian River Basin, designed to assess soil moisture controls on runoff generation under AR conditions. The observations consist of 2-minute volumetric soil moisture at 19 sites and 6 depths (5, 10, 15, 20, 50, and 100 cm), starting in summer 2017. The goals of this monitoring network are to aid the development of research applications and situational awareness tools for Forecast-Informed Reservoir Operations at Lake Mendocino. We present short analyses of these data to demonstrate their capability to characterize soil moisture responses to precipitation across sites and depths, including time series analysis, correlation analysis, and identification of soil saturation thresholds that induce runoff. Our results show strong inter-site Pearson's correlations (>0.8) at the seasonal timescale. Correlations are strong (>0.8) during events with high antecedent soil moisture and during drydown periods, and weak (<0.5) otherwise. High event runoff ratios are observed when antecedent soil moisture thresholds are exceeded, and when antecedent runoff is high. Although local heterogeneity in soil moisture can limit the utility of point source data in some hydrologic model applications, our analyses indicate three ways in which soil moisture data are valuable for model design: (1) sensors installed at 6 depths per location enable us to identify the soil depth below which evapotranspiration and saturation dynamics change, and therefore choose model soil layer depths, (2) time series analysis indicates the role of soil moisture processes

in controlling runoff ratio during precipitation, which hydrologic models should replicate, and (3) spatial correlation analysis of the soil moisture fluctuations helps identify when and where distributed hydrologic modeling may be beneficial.

Keywords

Atmospheric river, correlation analysis, hydrologic model evaluation, precipitation, Russian River Basin, soil moisture, streamflow, time series

1. Introduction

Atmospheric rivers (ARs) are concentrated bands of water vapor transport in the lower atmosphere, which cause heavy and sustained precipitation upon landfall. In California, 10-50% of precipitation occurs during AR events (Dettinger, Ralph, Das, Neiman, & Cayan, 2011; Kim et al., 2013), and some strong AR events drive floods, debris flows and associated damages (Corringham, Ralph, Gershunov, Cayan, & Talbot, 2019; Young, Skelly, & Cordeira, 2017). Therefore, accurate forecasting of ARs and their hydrologic impacts is essential for reservoir operations and flood control. Recognition of forecast value is leading to greater adaptivity in reservoir management, such that reservoirs are maintained at a higher base level, but drawn down in advance of incoming storms (Miao, Chen, & Hossain, 2016; Jasperse et al., 2017; Ralph, Jasperse, Talbot, & Wilson, 2019; Talbot, Ralph, & Jasperse, 2019).

For large-scale hydrologic modeling, such as for reservoir inflow forecasting, spatially distributed models are a popular choice (Archfield et al., 2015). These models represent hydrologic processes at the land surface, in soils, groundwater, and in the stream network. Soil moisture strongly controls runoff from the land surface into streams. Quantitative measurements of this soil

moisture control are vital to forecast runoff in regions where flooding is often caused by a single extreme precipitation event (Berghuijs, Woods, Hutton, & Sivapalan, 2016), such as California (Cao, Mehran, Ralph, & Lettenmaier, 2019). Multiple studies show soil saturation can quickly trigger runoff generation (e.g., Penna, Tromp-van Meerveld, Gobbi, Borga, & Dalla Fontana, 2011), and spatial correlations in soil moisture modify the hydrologic response at the watershed scale (McMillan, 2012; Western et al., 2004). Modeling and observational studies in California showed that wetter antecedent soil moisture conditions resulted in higher runoff ratios (Cao et al., 2019; Ralph, Coleman, Neiman, Zamora, & Dettinger, 2013).

Despite the importance of accurate representation of soil moisture, model calibration typically only uses meteorological variables and gauged flow data. Unlike precipitation (e.g., Schaake, Henkel, & Cong, 2004; Willie et al., 2017), soil moisture information is less frequently used in models because measurements are often sparse and values are too heterogeneous for meaningful comparisons between point measurements and distributed hydrologic models (Branger & McMillan, 2019). However, Pathiraja, Westra, & Sharma (2012) showed that design flood events were underestimated when antecedent soil moisture was not properly simulated. This problem is exacerbated by the scarcity of deep subsurface soil moisture measurements (> 50 cm), such that a surplus or deficit in soil moisture that controls hydrologic responses cannot be effectively characterized (Curtis, Flint, & Stern, 2019).

This paper presents a new and publicly available dataset collected in near real time, i.e., collected and made available within an hour. The dataset is collected from a denser network installed in the Russian River Basin in Northern California, to inform reservoir operations in the Lake Mendocino Sub-basin. The goals of this network are to: 1) improve soil moisture representation in distributed hydrologic model forecasts under AR conditions, 2) improve overall

monitoring of the soils in the watershed for situational awareness (as in Hatchett et al., 2020), and 3) advance our process-based understanding of the role of soils in the water cycle in this basin. This paper focuses on the first goal and highlights the value of spatially and temporally dense observations. To assess this network in that context, we first describe the impact of temporal and spatial patterns of soil moisture on runoff generation during AR events. The aim of this analysis is to recommend which features of the soil moisture response should be reproduced by a distributed model, for accurate forecasting of runoff volume.

2. CW3E Soil Moisture Observation Network

2.1. Network Description

The soil moisture monitoring network was installed in summer and fall 2017 as part of a wider Center for Western Weather and Water Extremes (CW3E) network of hydrometeorological instrumentation that supports research, operations, and situational awareness objectives in California. Among other parameters, the CW3E network monitors soil moisture, precipitation, and streamflow primarily in the Lake Mendocino watershed, a sub-basin of the Russian River watershed (Figure 1). A dense monitoring network is an essential component of Lake Mendocino Forecast-Informed Reservoir Operations (FIRO; Jasperse et al., 2017).

This study also incorporates soil moisture and precipitation data from the National Oceanic and Atmospheric Administration Earth System Research Laboratory (NOAA ESRL) Hydrometeorology Testbed (HMT), a national program focused on providing access to complementary datasets to enhance weather and water forecasts and accelerate the transition of cutting-edge research into operations. These networks are a part of the Russian River Hydrometeorological Observation Network (RHONET; described in detail in Sumargo et al.,

2020a). Data from the CW3E network are ingested in near real time in the NOAA Physical Science Division (PSD) data repository, in the Meteorological Assimilation Data Ingest System (MADIS), and in the California Data Exchange Center (CDEC).

The RHONET soil moisture monitoring network used probe types and installation methods consistent with the national HMT network (Zamora, Ralph, Clark, and Schneider, 2011). The CW3E network installation also considered the areas covered by five stream tributaries in the Lake Mendocino Sub-basin (Figure 1). Soil moisture is measured as volumetric water content (VWC)--volume of water measured in a unit volume of soil--using Campbell Scientific CS616 sensors (Campbell Scientific, Inc., 2016) at depths of 5, 10, 15, 20, 50, and 100 cm at 6 CW3E surface meteorological stations (Table 1). Depths were chosen to correspond with the pre-existing HMT network, which has 13 stations within the Russian River watershed (White et al., 2013). The availability of measurement from 5 cm to 100 cm provides a more comprehensive vertical profile of soil water storage, from shallow to root zone.

CW3E station locations were chosen to fill the gaps between the existing HMT stations and ensure representativeness in key soil parameters for hydrological modeling, including the Gridded Surface/Subsurface Hydrologic Analysis model (Downer & Ogden, 2004) and the National Water Model (Gochis et al., 2016), which are an integral part of FIRO. This was done by conducting a *k*-means cluster analysis (MacQueen, 1967) for 30-m grid cells in the Lake Mendocino watershed for the following parameters: slope; elevation; clay content; and silt content. Six clusters separated the watershed into the following types: (C1) flat and clay-rich; (C2) flat to moderate slopes with moderate clay content; (C3) steep slopes at middle elevations with moderate to high clay content; (C4) very sandy soils over various slopes and elevations; (C5) steep slopes at mid to upper elevations with very sandy soils; and (C6) high elevation steep slopes with moderate

clay content (Table S1 in the Supporting Information). Existing HMT sites covered the first two clusters, and the six CW3E sites, via partnerships with landowners and permits from the Bureau of Land Management and the USACE, were added to broaden the coverage to the four additional clusters (Table 1). During the siting visits and at installation, the field team surveyed the coordinates, slope angles, and elevations using the Theodolite tool (Hunter Research and Technology, LLC, 2009) and maps of soil parameters and topography (Figure S1 in the Supporting Information) in order to ensure the sites as well as the measurements were as representative as possible of the types of surrounding environment, topography, and soil makeup.

Precipitation, soil moisture, and other meteorological parameters measured at the six telemetered sites are recorded every two minutes and downloaded each hour. Stream stage data is manually downloaded from Solinst level loggers at CW3E stream gauges approximately twice per year and converted to discharge using rating curves. Soil moisture and streamflow data for this study undergo manual quality control that includes identifying gaps as well as flagging and removing questionable observations, i.e., outside a realistic range (0-1) or with improbable jumps between timestamps (a VWC increase of >10% between timestamps; Dorigo et al., 2013).

2.2. Soil Moisture Measurement Uncertainties

Any *in situ* hydrologic measurements involve uncertainties, including those related to measurement error and data treatment, which can propagate to the measurement values and reduce the information content of subsequent analyses (Westerberg & McMillan, 2015).

The CS616 soil moisture probe used by the CW3E network measures the dielectric permittivity of the soil to determine water content (Campbell Scientific, Inc., 2016). The manufacturer's specifications state that the probe does not require calibration for low-salinity soils

with saturated bulk electrical conductivity <0.5 dS/m and has a precision of better than 0.1% VWC and a water content accuracy of ±2.5% VWC using standard calibration with bulk electrical conductivity. Probe-to-probe variability is ±0.5% VWC in dry soil and ±1.5% in wet soil. Of greater concern is the potential for systematic errors. Tests of the CS616 probe show substantial influence of soil texture on the soil moisture measurements, leading to an estimate of uncertainty (root-mean-squared error) of 14% compared to gravimetric control measurements (Rüdiger et al., 2010). We therefore used ±14% as an estimate of the uncertainty in our soil moisture measurements. Soil moisture measurements are susceptible to further systematic error sources, such as flexing of the probe rods during installation, imperfect contact between the probes and soil, and measurement uncertainty related to the spatial heterogeneity in soil texture.

We therefore designed our analyses to be robust to systematic error sources, by normalizing the soil moisture data between wilting point and field capacity (Section 3.2). Using this normalization, our analyses of response time, saturation, diurnal cycles, thresholds and spatial correlation (Sections 3.3 to 3.7) are robust to multiplicative biases in the soil moisture values. However, the normalization would not be effective if biases exist that vary strongly with soil moisture magnitude. Soil moisture analyses have additional uncertainty due to missing values after sensor failure or where data is flagged during quality control. For our network the proportion of missing values was low (2.96%).

3. Methods

3.1. Precipitation and AR Event Identification

The start and end times of a precipitation (*P*) event often varies by minutes to ~1 hour even between sites within the same watershed. To simplify this problem, *P* events are identified using

mean-areal precipitation (MAP) (Figure 2)—defined as the average of six CW3E and three HMT stations located within the Lake Mendocino sub-basin. An event is defined as a period when precipitation (MAP > 0) occurs for at least 6 hours within the event duration, and when no precipitation gaps (MAP = 0) occur for more than 12 consecutive hours. Based on these criteria, 51 events occurred in water years (WYs) 2018-2019.

The AR events are identified using the bulk water vapor flux derived from wind and integrated water vapor (IWV) records from the Bodega Bay AR Observatory (ARO; White et al., 2013, Figure 1 upper left). The bulk water vapor flux is computed as follows:

$$Bulk\ WV\ Flux = IWV * \bar{U}_{750\text{-}1250} \quad (1)$$

where $\bar{U}_{750\text{-}1250}$ is the average total wind speed, regardless of direction, in the 750-1250m range of altitudes. This is the atmospheric layer most associated with rainfall at the nearby coastal mountains (Neiman, Ralph, White, Kingsmill, & Persson, 2002). To be classified as an AR, bulk water vapor flux is required to be at minimum 20 cm m s^{-1}, with an IWV value of at least 2 cm, for at least 8 consecutive hours (Ralph et al., 2013; Ralph et al., 2019a). The bulk water vapor flux is a proxy measurement for integrated vapor transport, the accepted quantity with which to identify ARs (e.g., Neiman, White, Ralph, Gottas, & Gutman, 2009; Smith, Yuter, Neiman, & Kingsmill, 2010; Hughes et al., 2014; Ralph et al., 2019b). Based on these criteria and the available ARO data, 26 of the 51 events in WYs 2018-2019 were AR events. (Note that 249 hours of ARO data were missing in the wet season (October-April) of WY 2018 and 1047 hours were missing in the wet season of WY 2019.)

3.2. Normalization of Soil Moisture Time Series

Soil moisture magnitudes are often locally variable and dependent on soil texture, even when dynamics are consistent, and therefore VWC normalization minimizes the impacts of VWC bias specific to the site. High soil moisture values (VWC > 0.6) at some locations (Figure 3) indicate possible issues related to the sensor environment or sensor malfunction. For instance, springs and inundated mudcracks have been observed near some locations, which may contribute to the high readings. Consequently, prior to our analyses, we normalize the soil moisture VWC between the permanent wilting point (VWC_{PWP}) and the field capacity (VWC_{FC}) in order to minimize the impacts of site-specific biases. The normalized VWC is determined as:

$$VWC_n = \frac{VWC - VWC_{PWP}}{VWC_{FC} - VWC_{PWP}} \qquad (2)$$

VWC_{FC} was identified as the secondary (higher) peak of the binned frequency distribution of bi-modal VWC, while VWC_{PWP} was identified as the lowest VWC on record. Physically, VWC_{FC} represents the amount of soil water storage after excess water has drained, while VWC_{PWP} represents the minimum soil water storage below which plants begin to wilt (Curtis et al., 2019).

3.3. Soil Moisture Response Time to Precipitation Event

Lag correlation analysis between local precipitation time series and VWC_n time series at different soil depths from 5 cm to 100 cm is conducted to assess the variation in soil moisture response time to precipitation across different soil depths. This analysis uses Pearson's correlation (Pearson, 1895), which measures the strength and direction of linear relationships between two time series. The lag correlation identifies the time lag between two time series that maximizes the cross-correlation (Yilmaz, Gupta, & Wagener, 2008), as one of the time series is shifted in time.

3.4. Diurnal Cycle of Soil Moisture

The presence of the diurnal cycle indicates the influence of external processes on the observed soil moisture fluctuations, particularly evapotranspiration (Jackson, 1973). We employ the Fourier Transform (FT) periodogram using Eisenman (2006) script—based on the discrete Fast FT algorithm (Frigo & Johnson, 1998)—to evaluate the strength of VWC fluctuations at different periods. For example, if a time series has a discernible spectral power at 24-hour period, typically with 30% more power than the neighboring frequencies/periods (Lundquist & Cayan, 2002), then the time series exhibits a diurnal cycle.

3.5. Cross-Depth Soil Moisture Saturations and T-Statistics

In a soil moisture time series, saturated soil moisture often appears as a persistent high VWC plateau. However, this plateau-like feature does not necessarily have a constant VWC value and may include small fluctuations. To account for this variability, we use a two-tiered percentile analysis to determine if the soil is saturated: 1) the VWC exceeds its all-time (WYs 2018-2019) 99^{th} percentile, or 2) the VWC exceeds its all-time 95^{th} percentile and its standard deviation at times t to t+24 hours is less than 0.1% of its all-time standard deviation. The saturation VWC identification is repeated for all 6 depths and 9 sites in the Lake Mendocino Sub-basin (Table 1).

Additionally, statistical tests are used to identify which depths show differences in soil moisture saturations. Here we compute the two-sample t-test to exemplify whether the population mean (μ) of saturation VWC at one depth and that at another depth are statistically distinct (Snedecor & Cochran, 1989; National Institute of Standards and Technology, 2012). Rejection of the null hypothesis (H_0) occurs when the samples do not provide sufficient evidence that the two populations are statistically distinct at the prescribed significance level, which in our case is at the 99% significance level (p-value < 0.01). A rejection of H_0 means the alternate hypothesis (H_a) is

favored, indicating that the two populations are statistically distinct. The test is repeated for different combinations: 5-cm VWC vs. 10-cm VWC, 5-cm VWC vs. 15-cm VWC, …., and 50-cm VWC vs. 100-cm VWC. We additionally conduct the test for: 1) all time VWCs, including saturation and non-saturation VWCs, 2) the all-time shallow-layer aggregate VWC (5-20 cm) vs. the deep-layer aggregate VWC (50-100 cm), and 3) the power spectra of VWCs, in order to verify the consistency in shallow layers vs. deep layers distinction. The computation is performed individually for the 9 CW3E and HMT sites in the Lake Mendocino Sub-basin.

3.6. Impact of Antecedent Soil Moisture on Event Runoff Ratio

We identify the impact of soil moisture and other antecedent conditions in our network as follows (Figure 3). Watersheds often display threshold behavior, which is characterized by a rapid increase in the event runoff coefficient (RC) after reaching a certain antecedent soil moisture value (Penna et al., 2011; McMillan et al., 2014). Event antecedent VWC_n was defined as the VWC_n prior to the start of the event. The event total runoff (R) from the nearest gauge is divided by the drainage area (A_D) and, subsequently, by the event total P to obtain the event RC:

$$RC = \frac{\sum_t \frac{R(t)}{A_D}}{\sum_t P(t)} \quad (3)$$

where t denotes the elapsed time within an event. Event antecedent VWC_n at each soil moisture sensor is then plotted against the RC for the nearest flow gauge (hereby threshold plot). Additional parameters, such as antecedent flow/runoff per unit drainage area (R_a), event total precipitation (P_{total}), and days from October 1st (the start of WY), can be added (e.g., as color codes) to the threshold plot to explore whether these parameters are related to the soil moisture vs. runoff relationship.

Additionally, we assess the strength of linear relationship between antecedent VWC_n and RC by computing the coefficient of determination (R^2) between RC and the linear fit ($\widehat{RC}$) of event antecedent VWC_n vs. RC. $\widehat{RC}$ is determined as:

$$\widehat{RC} = a * antecedent\ VWC_n + b \quad (4)$$

where *a* is the slope and *b* is the intercept. This computation is done for each site individually. The R^2 also indicates the amount of RC variance accounted for by the antecedent VWC_n.

3.7. Spatial Pattern Identification

The spatial correlation of RHONET soil moisture observations indicates the degree of covariance of soil moisture fluctuations across the basin, which controls the relationship between mean soil moisture and drainage (McMillan, 2012). We cross-correlate the 2-minute VWC at 10-cm depth at each of the six CW3E stations with all other stations in the Russian River Basin. Particularly, BCC is used as the baseline in our analysis due to the relatively low amount of missing data and its spatial representativeness in the watershed. The 10-cm depth is chosen because of its availability at all sites (Table 1) and its proximity to the surface—thereby minimizing the effect of local soil characteristics on the infiltration rate.

Pearson's correlation analysis (Pearson, 1895) is performed at different seasons to reveal the seasonal variations in the degree of co-variability: autumn (October–December), winter (January–March), spring (April–June), and summer (July–September). (Note that these seasons are tailored for WY format, which begins in October, and are offset from the traditional meteorological seasons.) Subsequently, the standard *N*-2 degrees of freedom (dof) associated with the Pearson's correlation is revised following Panofsky & Brier (1958) formulation to account for the presence of autocorrelation (Rai, 2019), which reduces the independent sample and affects the

significance value. This revision scales the dof with the *e*-folding time decay of the autocorrelation (T_e)—where autocorrelation drops to 1/*e*—such that:

$$dof = \frac{N*dt}{2*T_e} \quad (5)$$

where *N* is the sample size, dt is the time interval between data.

Additionally, the correlation analysis is performed at event time scales to investigate the spatial variation in soil moisture during and after events. The latter represents the drydown period responsible for setting up the antecedent soil moisture condition for the following event. To analyze event time scales, while minimizing the effects of higher-frequency (sub-daily to daily) fluctuations, soil moisture VWC_n is cross-correlated at ±7-day centered moving windows, such that:

$$CC(t) = \frac{N*\left(\sum_{t-7days}^{t+7days} VWC_n(x_1,z,t)*VWC_n(x_2,z,t)\right)-\left(\sum_{t-7days}^{t+7days} VWC_n(x_1,z,t)\right)*\left(\sum_{t-7days}^{t+7days} VWC_n(x_2,z,t)\right)}{\sqrt{\left(N*\sum_{t-7days}^{t+7days} VWC_n^2(x_1,z,t)-\left(\sum_{t-7days}^{t+7days} VWC_n(x_1,z,t)\right)^2\right)*\left(N*\sum_{t-7days}^{t+7days} VWC_n^2(x_2,z,t)-\left(\sum_{t-7days}^{t+7days} VWC_n(x_2,z,t)\right)^2\right)}} \quad (6)$$

where CC is the correlation coefficient, *N* denotes the sample size, *t* denotes a specific point in time in days, *z* denotes the soil depth, x_1 and x_2 denote sites 1 and 2, respectively. (Note that the correlation analyses described here are not intended to establish a causal relationship, but as a metric to determine whether the VWCs at the paired sites fluctuate in unison.)

4. Results and Discussion

4.1. Visualization of Soil Moisture Series

The time series of soil moisture at selected stations over a WY and during an atmospheric river event is useful to examine water dynamics and soil drainage (Figure 4). Boyes Creek Canyon (BCC), North Cow Mountain (NCM), and Potter Valley Central (pvc) are chosen to represent different environments existing in the basin, e.g., riparian (BCC), montane/hillslope (NCM), and valley (pvc). Soil moisture shows seasonal patterns of wetting and drying across different parts of

the Lake Mendocino Sub-basin and across the observed depths (Figures 4a-c). The plateaus at high VWC values during the wet seasons indicate soil saturation, as shown by the 100-cm VWCs of >0.6 at BCC (Figures 4a and 4d) and pvc (Figures 4c and 4f).

During a single event, the VWCs at different depths closely follow the precipitation (Figures 4d-f). Qualitatively, the responses from the shallow layers are virtually immediate, while those from the deep layers lag by several hours. Lag correlation analysis shows that the delay ranges from ~1 day to ~3 days, depending on the soil depth and the site. Averaged over 9 soil moisture observation sites in the Lake Mendocino Sub-basin and over 51 events in WYs 2018-2019, the delay ranges from ~2-3 hours at the near-surface layers (5-10 cm) to ~11 hours at the deepest layer (100 cm) (Figure 5). Deeper layers typically experience longer lags, since precipitation takes longer time to infiltrate the deeper layers. Similar features to those on Figures 4a-c are present, with saturation especially evident at deeper soil layers (50–100 cm).

The percentile analysis suggests that most sites exhibit much more frequent saturation at deep layers (50-100 cm) than at shallow layers (5-20 cm). For instance, the VWC profile at each of the 50-100-cm depths at BCC exhibits in total >1300 hours of saturation in WYs 2018-2019, while that at each of the 5-20-cm depths only exhibits in total <170 hours. An exception occurs at NCM, ptv, and pvw, whose time series exhibit infrequent persistent high VWC plateaus. The two-sample t-tests between different combinations of depths result in the rejections of H_0 with p-values <0.01 at most sites, except at pvw where only 50-cm and 100-cm depths result in the rejections of H0 when tested against the other depths. This result indicates that the VWC saturations at shallow layers and those at the deep layers are statistically distinct.

This difference between shallow- and deep-layer soil moisture is corroborated by the two-sample t-test of VWCs through the period of record, resulting in the rejection of H_0 with p-values

<<0.01 in all cases, except in the case of 15 cm vs. 50 cm at ptv. This outcome indicates the statistically distinct VWCs between one soil depth and another, except at ptv where the test suggests the lack of statistically distinct VWC characteristics between 15-cm and 50-cm depths. The test similarly results in the rejection of null hypothesis at all 9 sites in the Lake Mendocino Sub-basin when it is conducted between the shallow-layer aggregate (5-20 cm) and the deep-layer aggregate (50-100 cm).

These results demonstrate a clear differentiation between shallow soil moisture (5–20 cm) with infrequent saturation and deep soil moisture (50–100 cm) with persistent saturation. Furthermore, the power spectra of VWC exemplify discernible evapotranspiration-driven diurnal cycles at the shallow layer (10 cm) (Figure 6a), with diurnal spectral powers of at least 69% greater than those at the neighboring periods, but not at the deep layer (100 cm) (Figure 6b). The two-sample t-test conducted on the 10-cm and 100-cm VWC power spectra results in the rejection of H_0 at most sites with p-values <0.01, except at BCC (p-value = 0.62), confirming the statistical distinction between the two layers. However, the failure to reject H_0 at BCC merely reflects the similar population μ between the two layers, despite the lack of diurnal spectral power at 100-cm (Figure 6c). All things considered, this differentiation reflects the fact that shallow layers are more exposed to evapotranspiration--an important driver of soil moisture (Pathiraja et al., 2012) and its diurnal fluctuation (Jackson, 1973). In a model, this differentiation could be reproduced by using two soil layers, and evaluating for the difference in dynamics between the two.

4.2. Impact of Antecedent Soil Moisture on Event Runoff Ratio

Most locations in the Lake Mendocino Sub-basin exhibit rapid runoff responses when the antecedent soil moisture exceeds certain threshold values (Figure 7). This threshold behavior is

characterized by the antecedent VWC_n values at which RCs begin to increase rapidly, which are typically ~0.9-1 (Figures 3 and 7). For instance, averaged over the five sites shown in Figure 7, the mean RC associated with antecedent VWC_n of >1 is ~2.6 times greater than that associated with antecedent VWC_n of <1. The VWC_n threshold values of ~0.9–1 correspond to the VWC_{FC} (Equation 2), above which water drains through the soil under gravity (Figure 7) and the soil wetting-up and runoff generation are accelerated (Calder et al., 2002; Zotarelli, Dukes, & Morgan, 2010; McMillan, 2012). This range of threshold values is consistent with some other studies, which found minimal runoffs when the soil saturations were <70-80% (Penna et al., 2011; Radatz, Thompson, & Madison, 2013). However, some locations, such as NCM and WDG, do not exhibit clear threshold behaviors, as indicated by the low RCs virtually regardless of the antecedent VWC_n.

The moderate RCs at relatively dry antecedent VWC_n (e.g., some RCs are 0.3–0.6 at VWC_n of ~0.7 at BCC) and the low RCs at high antecedent VWC_n (e.g., some RCs are < 0.1 at VWC_n of > 1 at all sites) suggest that VWC_n and RC do not have a strong linear relationship ($R^2 < 0.16$ for all sites), even at VWC_n above the threshold values ($R^2 < 0.22$). For this reason, we consider other parameters that may control the soil moisture threshold behavior (Section 3.6), specifically the antecedent flow/runoff.

The color shadings in Figure 7 denote the R_a of each event in the record since the beginning of WY 2018. In the absence of precipitation, the antecedent runoff is equivalent to the baseflow. Baseflow principally comes from groundwater discharge (Wittenberg, 1999; Arnold, Muttiah, Srinivasan, & Allen, 2000), so the antecedent runoff is a proxy for groundwater levels and total antecedent catchment wetness (Beven, Leedal, Smith, & Young, 2012). This feature helps to explain why some events have high antecedent VWC_n (> 1) but low RC (< 0.2): these are typically

events with low R_a (<0.001 mm). Such events are notable at DRW and HDC, where 14 and 9 out of 51 events, respectively, fall into this category (Figure 7). Note that exceptions still exist for events with high antecedent soil moisture and flow, but low RC (e.g., at BCC, DRW): an inspection on the event dates reveal that these events are relatively small (with event P_{total} < median P_{total} for all 51 events) and occur late in the wet season (March-June). This analysis demonstrates the need for accurate representation of the groundwater relationship to soil moisture in hydrologic models, so events with significant antecedent soil moisture and groundwater influences can be accurately predicted.

4.3. Spatial Pattern Identification

4.3.1. Spatial correlation of soil moisture across the watershed

Cross-correlations of the 2-minute VWC time series at one site with the other sites in the Russian River Basin reveal spatial covariance of soil moisture fluctuations at a seasonal scale (Figure 8). In the example of cross-correlations at BCC, strong Pearson's correlations (> 0.6) with >99% statistical significance are observed at most sites for all seasons. Pearson's correlations are strongest in autumn and spring (> 0.8) when dry soils are wetting up, or wet soils are drying down, respectively. Correlations are weakest in winter, as soils are relatively wet throughout the basin, but have different VWC_{FC} and saturation levels. Consequently, the soil at one site may reach saturation more quickly than soil at another site during a storm event, especially since AR rainfall can vary across the basin (Cannon et al., 2020). Despite the varying correlation magnitudes, similar seasonal patterns are observed when the cross-correlations are performed at the other five CW3E stations (not shown), so the choice of site is trivial in this seasonal correlation analysis. This

similarity reflects the influence of precipitation on the seasonal soil moisture wet-up and dry-down processes in the watershed.

At the event timescale, strong VWC correlations throughout the basin are observed when the antecedent VWCs and event *P* total and/or intensity are also high, such as during the early April 2018 AR event (Hatchett, 2018) discussed in the following sub-section. While dynamics can diverge during inter-storm periods, cool-season precipitation events, particularly ARs, drive simultaneous soil moisture peaks across all sensors. Therefore, during AR events, soils throughout entire basins may reach runoff thresholds at similar times and have greater impacts on downstream water management operations and communities.

Similar patterns are observed at the other soil depths, with relatively comparable correlation magnitudes at shallow layers (5–20 cm) and low correlation magnitudes at deeper layers (50–100 cm; not shown). This cross-depth variation reflects the similarity of soil moisture behavior at the shallow layers as well as the presence of other factors in the deeper layers, such as the longer water infiltration time and the presence of bedrock (e.g., at NCM), springs (e.g., at HDC), or mudcracks (e.g., at DRW).

4.3.2. Event-scale spatial correlation of soil moisture

Soil moisture cross-correlations, which exhibit large swings associated with AR events, tend to converge at values > 0.8 during AR events, most notably during the February 28–March 4 (non-AR) and the April 5–8 (AR) events (Figure 9). These convergences coincide with very wet antecedent soil conditions (VWC_n > 1) at most sites. High-correlation convergence also occurs with prolonged drydown periods following some of the events, such as in late March–early April and mid–late April, when all sites exhibit soil moisture drying. In contrast, the correlations

decrease to < 0.5 shortly after the event cessations, such as around March 8, March 20, and April 15, particularly at the sites that are farther away from BCC (the reference site in Figure 9). This behavior occurs as the distinct environment at different sites dictate the lag and speed of soil moisture drainage following the events.

Overall, this analysis demonstrates that soil moisture fluctuations at event time scales are less uniform throughout the basin than the seasonal fluctuations (Figure 8). These fluctuations are site-specific, which reflects the value of dense soil moisture networks that capture a range of soil moisture responses during periods of frequent AR activity. During such periods, precipitation is a stronger controller of soil moisture behavior than evapotranspiration is (Cao et al., 2020), where early soil moisture recession characteristics shortly following the events set the antecedent conditions of the subsequent events.

5. Summary and Conclusions

We presented new and publicly available near real-time data from a soil moisture network across the Russian River Basin and Lake Mendocino Sub-basin in Northern California. The network was designed to improve soil moisture representation in distributed hydrologic model forecasts under extreme precipitation conditions, such as atmospheric rivers (ARs). The data underwent manual quality control to remove questionable values, and a normalization method was used to minimize the impacts of possible site-specific biases and uncertainties in applications, such as hydrologic model verification and flood forecasting.

Using the Fourier Transform periodogram and the two-sample t-test, we showed the different soil dynamics between the shallow layers (5-20 cm), with diurnal cycle, and the deep layers (50-100 cm), with relatively persistent soil saturation. We also found large increases in

runoff generation when the event antecedent soil moisture approached field capacity, above which the runoff coefficient was on average ~2.6 times greater. However, some events did not produce significant runoff despite the high antecedent soil moisture and heavy precipitation. Further analysis suggested a groundwater influence on runoff generation, where groundwater recharge may have reduced runoff and groundwater exfiltration may have increased runoff. Future studies should consider some other variables that may influence the soil moisture and runoff processes, such as event total precipitation, event average precipitation intensity, and air temperature.

We demonstrated lagged soil moisture responses with depth, from ~2-3 hours at near-surface layers (5-10 cm) to ~11 hours at the deepest layer (100 cm). We also showed strong site-to-site correlations of 2-minute soil moisture observations at seasonal scales, especially in response to ARs. This pattern indicated that precipitation was a dominant controller of seasonal soil moisture fluctuations throughout the Russian River Basin. However, these site-to-site correlations were highly variable at event time scales, depending on the distance between sites and antecedent soil conditions. Stronger correlations occurred when the time between two or more events was short, so the soil remained relatively wet through time and space (e.g., mid March 2018), and after event cessation during soil moisture recession (e.g., end of April 2018) (Figure 9).

These results demonstrated the ability of a high-resolution, multi-depth soil moisture observation network to capture the spatial and temporal soil moisture variabilities and consistencies throughout the Russian River Basin. Lessons that we drew from this analysis for hydrologic modeling in the watershed were that:

1) With multi-depth sensors, statistical tests can be used to identify which depths show differences in soil moisture dynamics (e.g., presence of saturation and diurnal cycles) and, therefore, should be used by modelers to define distinct model layers,

2) Understanding the factors that influence event runoff ratio during a precipitation event, such as soil moisture and antecedent runoff, enables us to design evaluation techniques, such as identifying the soil moisture threshold that induces runoff, and indicates soil moisture processes that distributed hydrologic models should replicate,
3) Analysis of decreases in soil moisture spatial correlation helps identify which areas of the watershed would benefit from a distributed calibration of model parameters related to soil moisture.

Ultimately, our findings emphasized the importance of a dense soil moisture monitoring network for monitoring and modeling runoff generation during extreme runoff events, and to ensure realistic representations of soil properties and heterogeneity, soil moisture/water drainage processes, and groundwater influence in hydrologic models.

Data Availability Statement

Soil moisture data as well as other raw data retrieved from CW3E's hydrometeorological network can be directly accessed in text format via the CW3E ftp data portal where they are continually updated in near real time (ftp://sioftp.ucsd.edu/CW3E_DataShare/CW3E_SurfaceMetObs/). Soil moisture and other raw data from HMT network can be accessed through a portal hosted by NOAA Earth Research and Science Laboratory's Physical Sciences Division (PSD; ftp://ftp1.esrl.noaa.gov/psd2/data/processed/SoilMoisture/). Additionally, NOAA PSD's Profiler Network Data and Image Library stores both CW3E and HMT data (https://www.esrl.noaa.gov/psd/data/obs/datadisplay/). The processed CW3E soil moisture, the raw and processed stream discharge data, and the stream rating curve information for this paper are available on Sumargo et al. (2020b) repository.

Supporting Information Legend

Supporting_Information_S1.docx: Cluster Analysis of Soil and Topography

References

Archfield, S. A., Clark, M., Arheimer, B., Hay, L. E., McMillan, H., Kiang, J. E., ... & Farmer, W. H. (2015). Accelerating advances in continental domain hydrologic modeling. *Water Resources Research*, *51*(12), pp.10078-10091.

Arnold, J. G., Muttiah, R. S., Srinivasan, R., & Allen, P. M. (2000). Regional estimation of base flow and groundwater recharge in the Upper Mississippi river basin. *Journal of Hydrology*, *227*(1-4), 21-40.

Berghuijs, W. R., Woods, R. A., Hutton, C. J., & Sivapalan, M. (2016). Dominant flood generating mechanisms across the United States. *Geophysical Research Letters*, *43*(9), 4382-4390.

Beven, K. J., Leedal, D. T., Smith, P. J., & Young, P. C. (2012). Identification and representation of state dependent non-linearities in flood forecasting using the DBM methodology. In *System identification, environmental modelling, and control system design* (pp. 341-366). Springer, London.

Branger, F., & McMillan, H. K. (2020). Deriving hydrological signatures from soil moisture data. *Hydrological Processes*, *34*, 1410– 1427. https://doi.org/10.1002/hyp.13645

Calder, I. R., Reid, I., Nisbet, T., Armstrong, A., Green, J. C., & Parkin, G. (2002). Study of the Potential Impacts on Water Resources of Proposed Afforestation. *Trees and Drought Project on Lowland England – TaDPoLE.* [Available at http://sciencesearch.defra.gov.uk/Document.aspx?Document=WT01008_2051_FRP.pdf]

Cannon, F., Oakley, N. S., Hecht, C. W., Michaelis, A., Cordeira, J. M., Kawzenuk, B., ... & Ralph, F. M. (2020). Observations and Predictability of a High-Impact Narrow Cold-Frontal Rainband over Southern California on 2 February 2019. *Weather and Forecasting*, 1-40, doi: https://doi.org/10.1175/WAF-D-20-0012.1.

Campbell Scientific, Inc. (2016). CS616 and CS625 Water Content Reflectometers: Instruction Manual. [Available at https://s.campbellsci.com/documents/af/manuals/cs616.pdf]

Cao, Q., Gershunov, A., Shulgina, T., Ralph, F. M., Sun, N., & Lettenmaier, D. P. (2020). Floods due to atmospheric rivers along the US West Coast: The role of antecedent soil moisture in a warming climate. *Journal of Hydrometeorology*, *21*(8), 1827-1845.

Cao, Q., Mehran, A., Ralph, F. M., & Lettenmaier, D. P. (2019). The role of hydrologic initial conditions on atmospheric river floods in the Russian River basin. *Journal of Hydrometeorology*, *20*(8), 1667-1686. doi:10.1175/JHM-D-19-0030.1.

Corringham, T. W., Ralph, F. M., Gershunov, A., Cayan, D. R., & Talbot, C.A. (2019). Atmospheric rivers drive flood damages in the western United States. *Science Advances*, *5*(12), p.eaax4631.

Curtis, J. A., Flint, L. E., & Stern, M. A. (2019). A Multi-Scale Soil Moisture Monitoring Strategy for California: Design and Validation. *JAWRA Journal of the American Water Resources Association*, *55*(3), 740–758, https://doi.org/10.1111/1752-1688.12744.

Dettinger, M. D., Ralph, F. M., Das, T., Neiman, P. J., & Cayan, D.R. (2011). Atmospheric rivers, floods and the water resources of California. *Water*, *3*(2), pp.445-478.

Dorigo, W. A., Xaver, A., Vreugdenhil, M., Gruber, A., Hegyiova, A., Sanchis-Dufau, A. D., ... & Drusch, M. (2013). Global automated quality control of in situ soil moisture data from the International Soil Moisture Network. *Vadose Zone Journal*, *12*(3).

Downer, C. W., & Ogden, F. L. (2004). GSSHA: Model to simulate diverse stream flow producing processes. *Journal of Hydrologic Engineering*, *9*(3), 161-174.

Eisenman, I. (2006). Create power spectrum estimate using either (i) periodogram, (ii) averaging over frequency bands, or (iii) Thompson multi-taper method. [Available at http://eisenman.ucsd.edu/code/matlab-toolbox/power_spectrum.m]

Frigo, M., & Johnson, S. G. (1998). FFTW: An adaptive software architecture for the FFT. In *Proceedings of the 1998 IEEE International Conference on Acoustics, Speech and Signal Processing, ICASSP'98 (Cat. No. 98CH36181)* (Vol. 3, pp. 1381-1384). IEEE.

Gochis, D., Dugger, A., McCreight, J., Karsten, L., Yu, W., Pan, L., …& Lee, H. (2016). Technical Description of the National Water Model Implementation WRF-Hydro. [Available at https://www.cuahsi.org/uploads/cyberseminars/wrf_hydro_nwm_cuahsi_nwm_webinar_oct_2016_%281%29.pdf]

Hatchett, B. J. (2018). Snow Level Characteristics and Impacts of a Spring Typhoon-Originating Atmospheric River in the Sierra Nevada, USA. *Atmosphere*, *9*(6), 233.

Hatchett, B. J., Cao, Q., Dawson, P. B., Ellis, C. J., Hecht, C. W., Kawzenuk, B., ... & Sumargo, E. (2020). Observations of an extreme atmospheric river storm with a diverse sensor network. *Earth and Space Science*, *6*, e2020EA001129, https://doi. org/10.1029/2020EA001129

Hughes, M., Mahoney, K. M., Neiman, P. J., Moore, B. J., Alexander, M., & Ralph, F. M. (2014). The landfall and inland penetration of a flood-producing atmospheric river in Arizona. Part II: Sensitivity of modeled precipitation to terrain height and atmospheric river orientation. *Journal of Hydrometeorology*, *15*(5), 1954-1974.

Hunter Research and Technology, LLC (2009). THEODOLITE: The original, indispensable, pioneering AR viewfinder. [Available at http://hunter.pairsite.com/theodolite/]

Jackson, R. D. (1973). Diurnal changes in soil water content during drying. *Field soil water regime*, *5*, 37-55.

Jasperse, J., Ralph, M., Anderson, M., Brekke, L. D., Dillabough, M., Dettinger, M. D., ... & Webb, R. H. (2017). *Preliminary viability assessment of Lake Mendocino forecast informed reservoir operations*. Center for Western Weather and Water Extremes.

Kim, J., Waliser, D. E., Neiman, P. J., Guan, B., Ryoo, J. M., & Wick, G.A. (2013). Effects of atmospheric river landfalls on the cold season precipitation in California. *Climate dynamics*, *40*(1-2), pp.465-474.

Lundquist, J. D., & Cayan, D. R. (2002). Seasonal and spatial patterns in diurnal cycles in streamflow in the western United States. *Journal of Hydrometeorology*, *3*(5), 591-603.

MacQueen, J. (1967, June). Some methods for classification and analysis of multivariate observations. In *Proceedings of the fifth Berkeley symposium on mathematical statistics and probability* (Vol. 1, No. 14, pp. 281-297).

McMillan, H. K. (2012). Effect of spatial variability and seasonality in soil moisture on drainage thresholds and fluxes in a conceptual hydrological model. *Hydrological Processes*, *26*(18), 2838-2844.

McMillan, H., Gueguen, M., Grimon, E., Woods, R., Clark, M., & Rupp, D. E. (2014). Spatial variability of hydrological processes and model structure diagnostics in a 50 km2 catchment. *Hydrological Processes*, *28*(18), 4896-4913.

Miao, Y., Chen, X., & Hossain, F. (2016). Maximizing hydropower generation with observations and numerical modeling of the atmosphere. *Journal of Hydrologic Engineering*, *21*(6), p.02516002.

National Institute of Standards and Technology (2012). Two-Sample t-Test for Equal Means. *NIST-SEMATECH Engineering Statistics Handbook*. [Available at https://www.itl.nist.gov/div898/handbook/eda/section3/eda353.htm#:~:text=The%20two%2Dsample%20t%2Dtest,two%20population%20means%20are%20equal.&text=For%20paired%20samples%2C%20the%20difference,or%20may%20not%20be%20equal.].

Neiman, P. J., Ralph, F. M., White, A. B., Kingsmill, D. E., & Persson, P. O. G. (2002). The statistical relationship between upslope flow and rainfall in California's coastal mountains: observations during CALJET. *Monthly Weather Review*, *130*, 1468–1492.

Neiman, P. J., White, A. B., Ralph, F. M., Gottas, D. J., & Gutman, S. I. (2009, April). A water vapour flux tool for precipitation forecasting. In *Proceedings of the Institution of Civil Engineers-Water Management*, *162*, 83-94, https://doi.org/10.1680/wama.2009.162.2.83.

Panofsky, H. A., & Brier, G. W. (1958). Some applications of statistics to meteorology. Mineral Industries Extension Services, College of Mineral Industries, Pennsylvania State University.

Pathiraja, S., Westra, S., & Sharma, A. (2012). Why continuous simulation? The role of antecedent moisture in design flood estimation. *Water Resources Research*, *48*, W06534, doi:10.1029/2011WR010997.

Pearson, K. (1895). Notes on regression and inheritance in the case of two parents. *Proc. Roy. Soc. London*, *58*, 240–242, doi:https://doi.org/10.1098/rspl.1895.0041.

Penna, D., Tromp-van Meerveld, H. J., Gobbi, A., Borga, M., & Dalla Fontana, G. (2011). The influence of soil moisture on threshold runoff generation processes in an alpine headwater catchment. *Hydrology and Earth System Sciences*, *15*(3), 689-702.

Radatz, T. F., Thompson, A. M., & Madison, F. W. (2013). Soil moisture and rainfall intensity thresholds for runoff generation in southwestern Wisconsin agricultural watersheds. *Hydrological Processes*, *27*(25), 3521-3534.

Rai, U. (2019). Estimation of the degrees of freedom for time series. [Available at https://iescoders.com/estimation-of-the-degrees-of-freedom-time-series/]

Ralph, F. M., Wilson, A. M., Shulgina, T., Kawzenuk, B., Sellars, S., Rutz, J. J., Lamjiri, M. A., Barnes, E. A., Gershunov, A., Guan, B., Nardi, K. M., Osborne, T., & Wick, G. A., (2019a). ARTMIP-early start comparison of atmospheric river detection tools: how many atmospheric rivers hit northern California's Russian River watershed? *Climate Dynamics*, *52*, 4973-4994.

Ralph, F. M., Rutz, J. J., Cordeira, J. M., Dettinger, M., Anderson, M., Reynolds, D., Schick, L. J., & Smallcomb, C. (2019b). A Scale to Characterize the Strength and Impacts of Atmospheric Rivers. *Bull. Amer. Meteor. Soc.*, *100*(2), 269-289.

Ralph, F. M., Coleman, T., Neiman, P. J., Zamora, R. J., & Dettinger, M. D. (2013). Observed Impacts of Duration and Seasonality of Atmospheric-River Landfalls on Soil Moisture and Runoff in Coastal Northern California. *Journal of Hydrometeorology*, *14*, 443–459, https://doi.org/10.1175/JHM-D-12-076.1

Ralph, F. M., Jasperse, J., Talbot, C. A., & Wilson, A. M. (2019). Forecast informed reservoir operations: Developing best practices for enhancing use of existing water management infrastructure. SEDHYD2019, Reno, NV, US Army Corps of Engineers

Rüdiger, C., Western, A. W., Walker, J. P., Smith, A. B., Kalma, J. D., & Willgoose, G. R. (2010). Towards a general equation for frequency domain reflectometers. *Journal of Hydrology*, *383*(3-4), pp.319-329.

Schaake, J., Henkel, A., & Cong, S. (2004). Application of prism climatologies for hydrologic modeling and forecasting in the western U.S. *Proc. 18th Conf. on Hydrology*, Seattle, WA, Amer. Meteor. Soc., 5.3. [Available online at http:// ams.confex.com/ams/pdfpapers/72159.pdf.]

Smith, B. L., Yuter, S. E., Neiman, P. J., & Kingsmill, D. E. (2010). Water vapor fluxes and orographic precipitation over northern California associated with a landfalling atmospheric river. *Monthly Weather Review*, *138*(1), 74-100.

Snedecor, G. W., & Cochran, W. G. (1989). Statistical methods, 8thEdn. *Ames: Iowa State Univ. Press Iowa*, *54*, 71-82.

Sumargo, E., McMillan, H., Weihs, R., Ellis, C. J., Wilson, A. M., & Ralph, F. M. (2020b). Data from: A Soil Moisture Monitoring Network to Assess Controls on Runoff Generation During Atmospheric River Events. *UC San Diego Library Digital Collections*. https://doi.org/10.6075/J0SN07G9

Sumargo, E., Wilson, A. M., Ralph, F. M., Weihs, R., White, A., Jasperse, J., ... & Delle Monache, L. (2020a). The Hydrometeorological Observation Network in California's Russian River Watershed: Development, Characteristics and Key Findings from 1997 to 2019. *Bulletin of the American Meteorological Society*, doi: https://doi.org/10.1175/BAMS-D-19-0253.1.

Talbot, C. A., Ralph, F. M., & Jasperse, J. (2019). Forecast-Informed Reservoir Operations: Lessons Learned from a Multi-Agency Joint Research and Operations Effort. *Federal Interagency Sedimentation and Hydrologic Modeling Conference*, June 25-28, Reno, Nevada. Conference Proceeding.

Westerberg, I. K., & McMillan, H. K. (2015). Uncertainty in hydrological signatures. *Hydrology and Earth System Sciences*, *19*(9), 3951-3968, doi:10.5194/hess-19-3951-2015.

Western, A. W., Zhou, S. L., Grayson, R. B., McMahon, T. A., Bloschl, G., & Wilson, D. J. (2004). Spatial correlation of soil moisture in small catchments and its relationship to dominant spatial hydrological processes. *Journal of Hydrology*, *286*(1–4): 113–134.

White, A. B., Anderson, M. L., Dettinger, M. D., Ralph, F. M., Hinojosa, A., Cayan, D. R., ... & Cifelli, R. (2013). A Twenty-First-Century California observing network for monitoring extreme weather events. *Journal of Atmospheric and Oceanic Technology*, *30*, 1585-1603, doi:10.1175/JTECH-D-12-00217.1

Willie, D., Chen, H., Chandrasekar, V., Cifelli, R., Campbell, C., Reynolds, D., ... & Zhang, Y. (2017). Evaluation of multisensor quantitative precipitation estimation in Russian River Basin. *Journal of Hydrologic Engineering*, *22*(5), E5016002.

Wittenberg, H. (1999). Baseflow recession and recharge as nonlinear storage processes. *Hydrological Processes*, *13*(5), 715-726.

Yilmaz, K. K., Gupta, H. V., & Wagener, T. (2008). A process-based diagnostic approach to model evaluation: Application to the NWS distributed hydrologic model. *Water Resources Research*, *44*, W09417.

Young, A. M., Skelly, K. T., & Cordeira, J. M. (2017). High-impact hydrologic events and atmospheric rivers in California: An investigation using the NCEI Storm Events Database. *Geophysical Research Letters*, *44*(7), pp.3393-3401.

Zamora, R. J., Ralph, F. M., Clark, E., & Schneider, T. (2011). The NOAA Hydrometeorology Testbed soil moisture observing networks: Design instrumentation, and preliminary results. *Journal of Atmospheric and Oceanic Technology*, *28*(9), 1129–1140, https://doi.org/10.1175/2010JTECHA1465.1

Zotarelli, L., Dukes, M. D., & Morgan, K. T. (2010). Interpretation of soil moisture content to determine soil field capacity and avoid over-irrigating sandy soils using soil moisture sensors. *AE460. (University of Florida Institute of Food and Agricultural Sciences: Gainesville, FL.).*

Table 1. A list of the 6 CW3E and 13 HMT surface meteorological stations monitoring soil moisture in the Russian River Basin, with the soil clusters for the 6 CW3E and 3 HMT stations in the Lake Mendocino Sub-basin (boldface station IDs) included.

Station	ID	Network	Latitude (°)	Longitude (°)	Elevation (m)	Period	Soil Cluster	Soil Depth Availability					
								5 cm	10 cm	15 cm	20 cm	50 cm	100 cm
Boyes Creek Canyon	**BCC**	CW3E	39.3405	-123.1635	317	2017-present	C5	✓	✓	✓	✓	✓	✓
Deerwood	**DRW**		39.1977	-123.1599	280	2017-present	C2	✓	✓	✓	✓	✓	✓
Hell's Delight Canyon	**HDC**		39.2686	-123.1486	646	2017-present	C5	✓	✓	✓	✓	✓	✓
North Cow Mountain	**NCM**		39.1796	-123.08	1031	2017-present	C4	✓	✓	✓	✓	✓	✓
Potter Valley North	**PVN**		39.3613	-123.1132	420	2017-present	C4	✓	✓	✓	✓	✓	✓
Windy Gap	**WDG**		39.2344	-123.0049	834	2017-present	C3	✓	✓	✓	✓	✓	✓
Cazadero	czc	HMT	38.6107	-123.2152	478	2005-present		✓	✓	✓	✓	✓	✓
Healdsburg	hbg		38.653	-122.8732	70	2006-present			✓	✓		✓	
Hopland	hld		39.003	-123.1209	164	2010-present			✓	✓		✓	
Lake Sonoma	lsn		38.7187	-123.0537	396	2010-present			✓	✓		✓	
Middletown	mdt		38.7456	-122.7112	972	2016-present		✓	✓	✓	✓		
Potter Valley	**ptv**		39.3357	-123.1383	303	2011-present	C2		✓	✓		✓	
Potter Valley Central	**pvc**		39.3209	-123.1028	289	2016-present	C1	✓	✓	✓	✓	✓	✓
Potter Valley West	**pvw**		39.3204	-123.1802	518	2016-present	C2	✓	✓	✓	✓	✓	✓
Rio Nido	rod		38.5073	-122.9565	39	2006-present			✓	✓		✓	
Redwood Valley East	rve		39.3143	-123.1869	520	2016-present		✓	✓	✓	✓	✓	✓
Redwood Valley North	rvn		39.3406	-123.2297	294	2016-present		✓	✓	✓	✓	✓	✓
Redwood Valley West	rvw		39.3014	-123.2601	631	2016-present		✓	✓	✓	✓	✓	✓
Willits	wls		39.3463	-123.3166	594	2010-present			✓	✓		✓	

Figure Legends

Figure 1. Terrain base maps showing the locations of RHONET soil moisture observations (left), including the HMT and CW3E stations within the Lake Mendocino Sub-basin (right). Also shown is a California map with pointers on Russian River Basin and Bodega Bay ARO site (top left inset). The CW3E and United States Geological Survey (USGS) stream gauges are also shown, which are parts of the RHONET in the greater Russian River Basin as well as within the Lake Mendocino sub-basin. Orange contours delineate areas that drain into five CW3E stream gauges.

Figure 2. Lake Mendocino sub-basin MAP time series from October to May of WY 2019, with AR events shaded in gray.

Figure 3. An illustration of a framework for identifying soil moisture threshold behavior, using soil moisture VWC_n at BCC and runoff per unit area derived from the nearby BYS stream discharge. The precipitation event numbers are based on the WYs 2018–2019 record. The threshold, as approximated by the vertical black line, is the soil moisture value at which runoff generation becomes efficient. Different arrow line types denote different segments of the process: Segment 1 denotes the VWC normalization; Segment 2 denotes the precipitation event identification; Segment 3 denotes the runoff coefficient computation.

Figure 4. Left: WYs 2018–2019 soil moisture VWC time series at BCC, NCM, and pvc sites at 6 different depths, representing riparian, montane, and valley environment, respectively. Right: April 2018 9-station mean precipitation (gray bars) and VWC (colored lines) time series at the same stations and depths as in a-c. The dashed-line boxes demarcate the April 2018 period.

Figure 5. Lag correlations between precipitation and VWC at 9 CW3E and HMT sites in the Lake Mendocino Sub-basin (color lines), averaged over 51 precipitation events in WYs 2018-2019, with the 9-site average plotted in thick black line. Time lags > 0 indicate the delay in VWC response. Different panels represent different soil depths, from 5 cm (top) to 100 cm (bottom). The vertical lines denote the time lag at which the maximum correlations for the 9-site average occur.

Figure 6. (a) FT power spectra of 10-cm VWCs (representing shallow soil layers) at 9 sites in the Lake Mendocino Sub-basin, showing the strength of VWC fluctuations at diurnal (24 hours) and event/synoptic (71-168 hours) time scales. The individual sites are plotted in pastel colors, while the 9-site averages are plotted in bold colors. (b) Same as (a), except for 100-cm VWC (representing deep soil layers). (c) FT power spectra of the 10-cm and 100-cm VWCs at BCC.

Figure 7. Event antecedent soil moisture VWC_n vs. RC plots at 5 different stations where both soil moisture and stream observations are available: (a) BCC, (b) DRW, (c) HDC, (d) NCM, and (e) WDG. Color shading represents antecedent runoff per unit area based on each associated stream gauge, showing the variability across sites of soil moisture threshold behavior and its relationship to antecedent runoff, a groundwater proxy.

Figure 8. Pearson's correlation maps of 2-minute soil moisture VWC_n with BCC site at 10-cm depth for (a) autumn (Oct–Dec), (b) winter (Jan–Mar), (c) spring (Apr–Jun), and (d) summer (Jul–Sep) of WYs 2018-2019. The thick black contours demarcate the Lake Mendocino Sub-basin. The

sites where the correlations are statistically significant at 99% significance level are outlined in black.

Figure 9. Mid February–April 2018 time series of (a) hourly precipitation, (b) 2-minute soil moisture VWC_n at 10-cm depth, and (c) ±7-day centered cross-correlations of 2-minute soil moisture VWC_n at 10-cm depth with the BCC site. The gray shadings demarcate AR periods. The plot colors on the middle and bottom panel denote site distances from BCC.

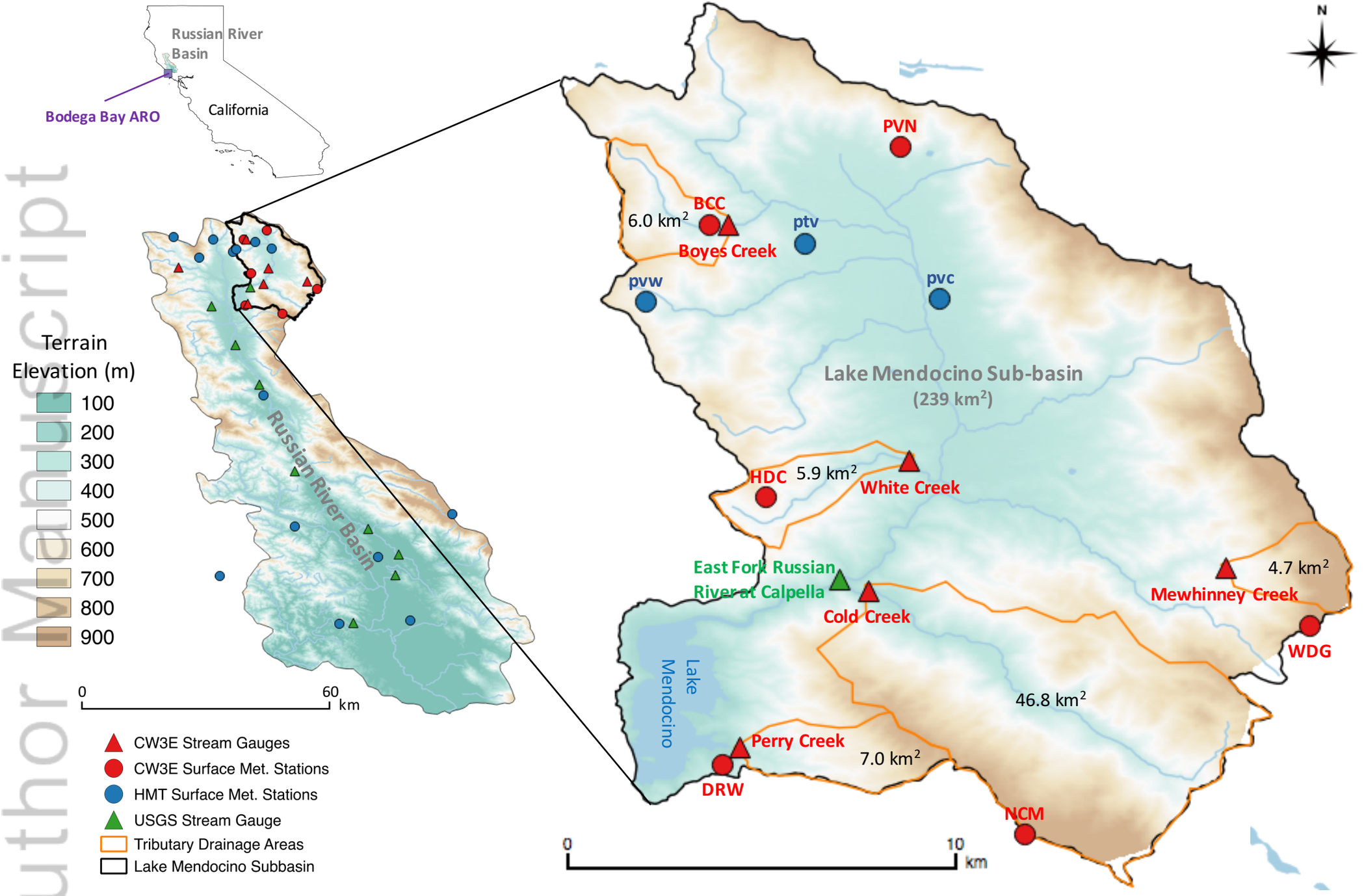

Figure 1. Terrain base maps showing the locations of RHONET soil moisture observations (left), including the HMT and CW3E stations within the Lake Mendocino Sub-basin (right). Also shown is a California map with pointers on Russian River Basin and Bodega Bay ARO site (top left inset). The CW3E and United States Geological Survey (USGS) stream gauges are also shown, which are parts of the RHONET in the greater Russian River Basin as well as within the Lake Mendocino sub-basin. Orange contours delineate areas that drain into five CW3E stream gauges.

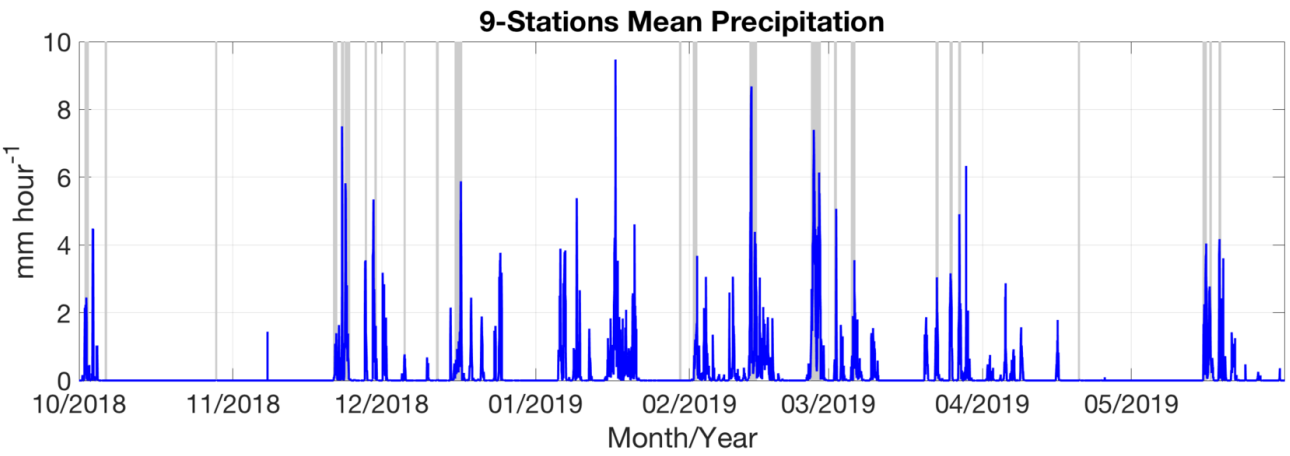

HYP_13998_Figure2.tiff

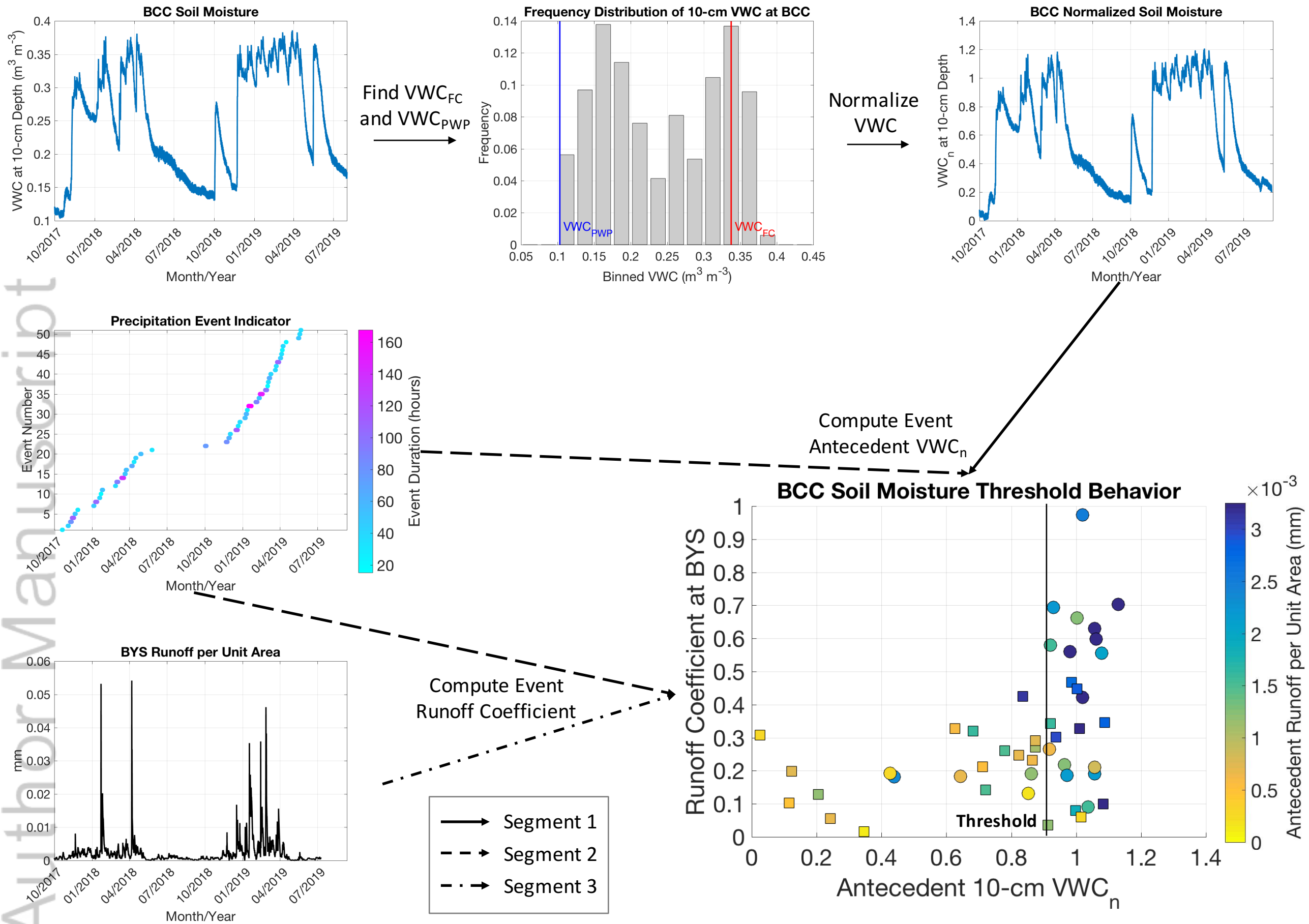

Figure 3. An illustration of a framework for identifying soil moisture threshold behavior, using soil moisture VWC_n at BCC and runoff per unit area derived from the nearby BYS stream discharge. The precipitation event numbers are based on the WYs 2018–2019 record. The threshold, as approximated by the vertical black line, is the soil moisture value at which runoff generation becomes efficient. Different arrow line types denote different segments of the process: Segment 1 denotes the VWC normalization; Segment 2 denotes the precipitation event identification; Segment 3 denotes the runoff coefficient computation.

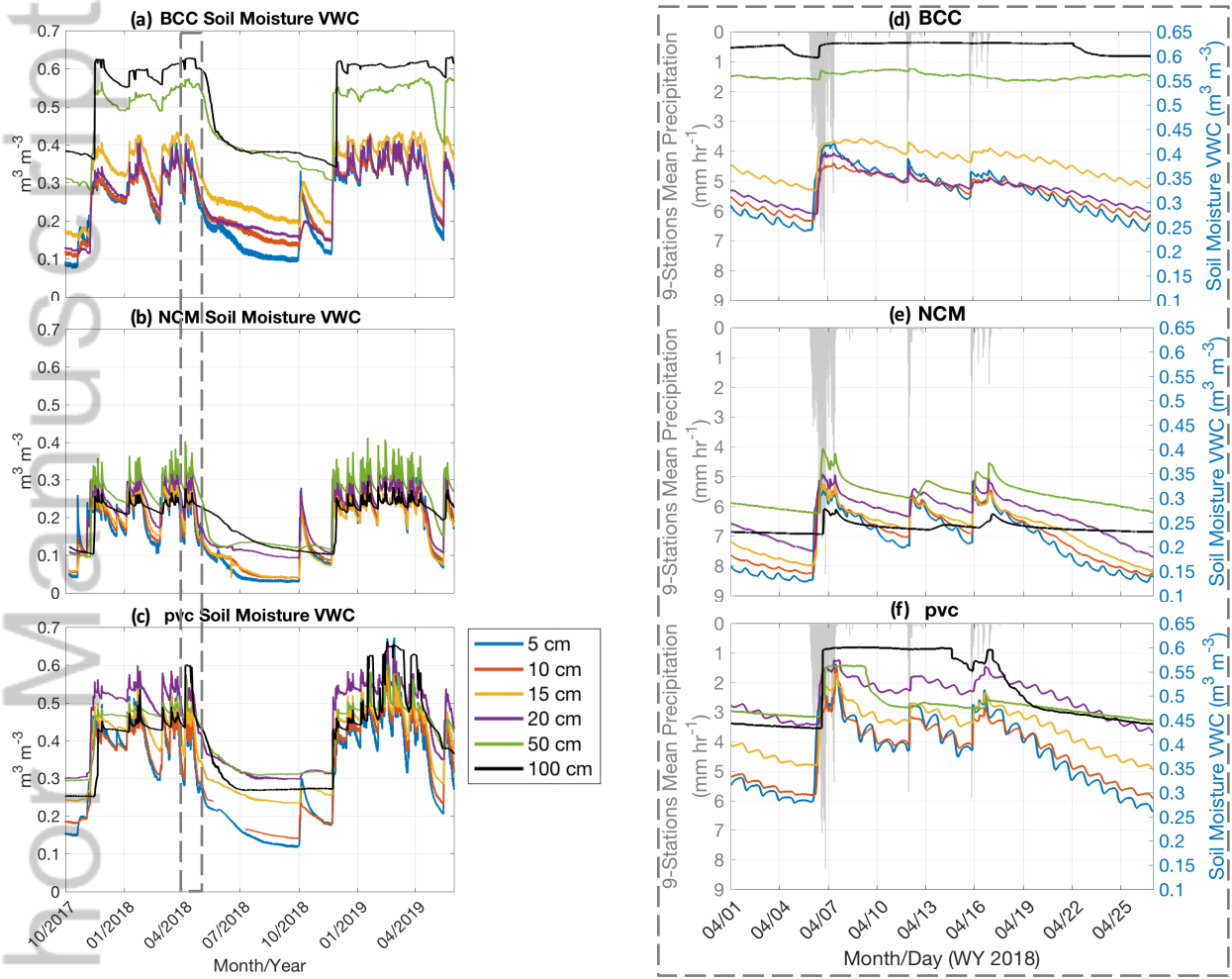

Figure 4. Left: WYs 2018–2019 soil moisture VWC time series at BCC, NCM, and pvc sites at 6 different depths, representing riparian, montane, and valley environment, respectively. Right: April 2018 9-station mean precipitation (gray bars) and VWC (colored lines) time series at the same stations and depths as in a-c. The dashed-line boxes demarcate the April 2018 period.

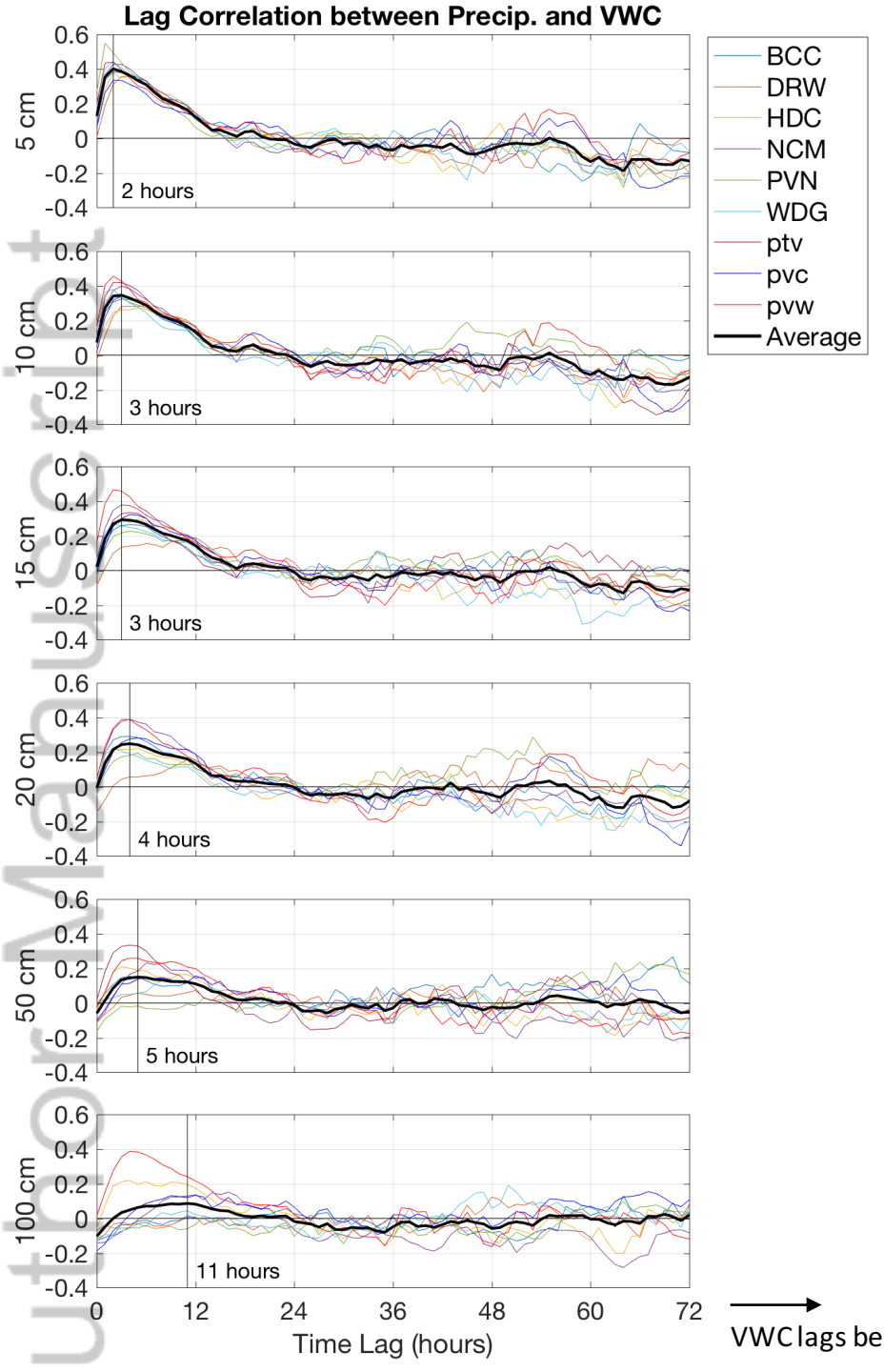

Figure 5. Lag correlations between precipitation and VWC at 9 CW3E and HMT sites in the Lake Mendocino Sub-basin (color lines), averaged over 51 precipitation events in WYs 2018-2019, with the 9-site average plotted in thick black line. Time lags > 0 indicate the delay in VWC response. Different panels represent different soil depths, from 5 cm (top) to 100 cm (bottom). The vertical lines denote the time lag at which the maximum correlations for the 9-site average occur.

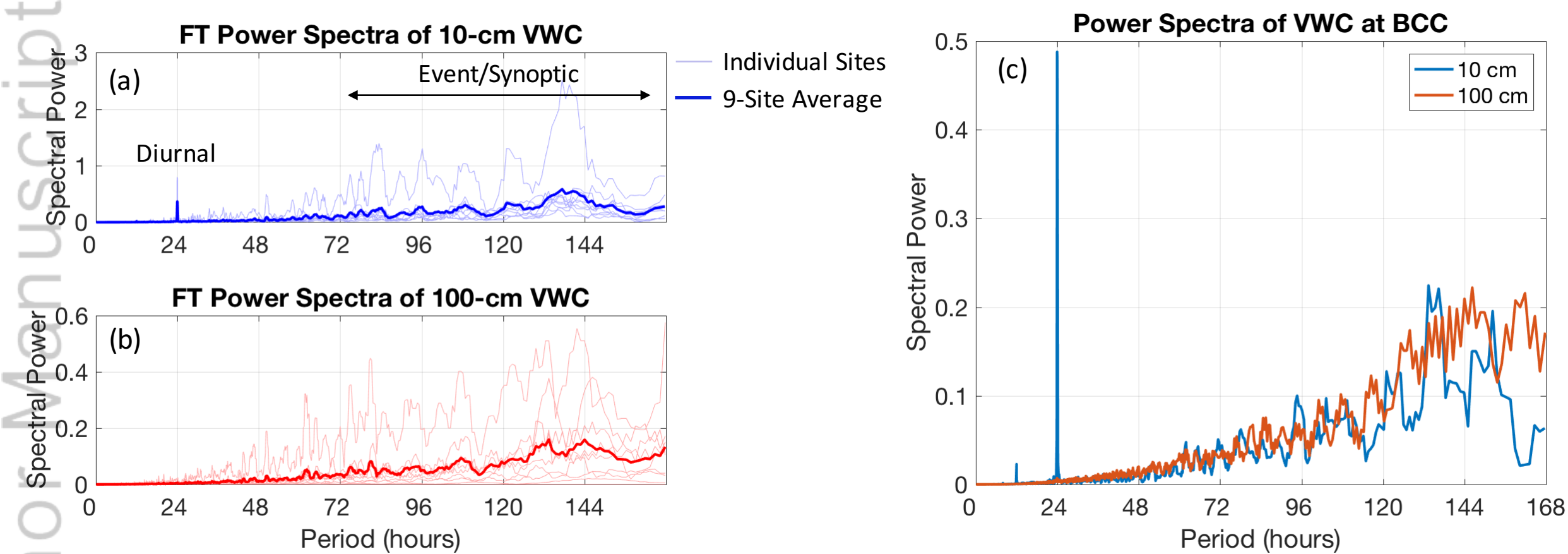

Figure 6. (a) FT power spectra of 10-cm VWCs (representing shallow soil layers) at 9 sites in the Lake Mendocino Sub-basin, showing the strength of VWC fluctuations at diurnal (24 hours) and event/synoptic (72-168 hours) time scales. The individual sites are plotted in pastel colors, while the 9-site averages are plotted in bold colors. (b) Same as (a), except for 100-cm VWC (representing deep soil layers). (c) FT power spectra of the 10-cm and 100-cm VWCs at BCC.

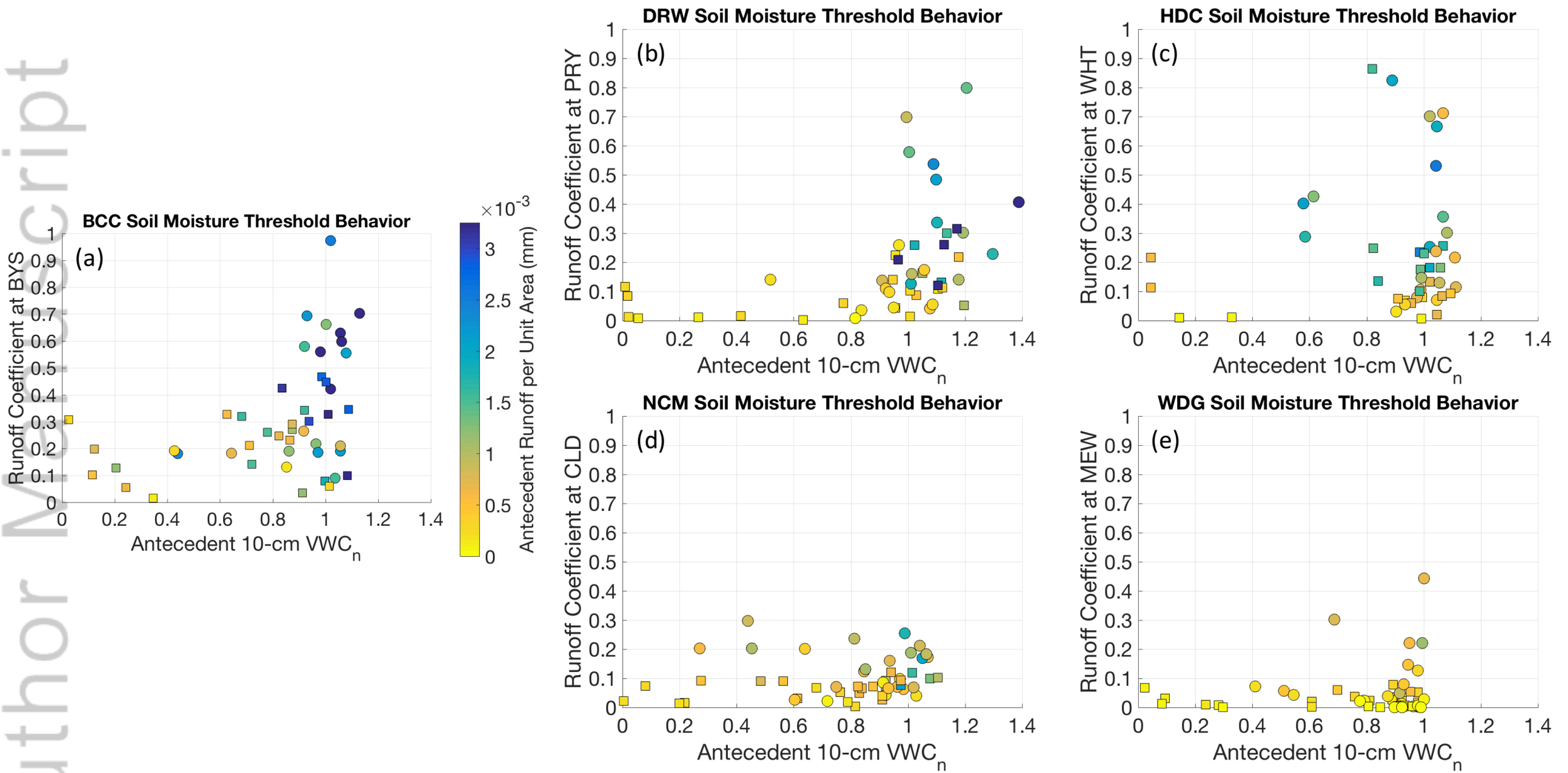

Figure 7. Event antecedent soil moisture VWC_n vs. RC plots at 5 different stations where both soil moisture and stream observations are available: (a) BCC, (b) DRW, (c) HDC, (d) NCM, and (e) WDG. Color shading represents antecedent runoff per unit area based on each associated stream gauge, showing the variability across sites of soil moisture threshold behavior and its relationship to antecedent runoff, a groundwater proxy.

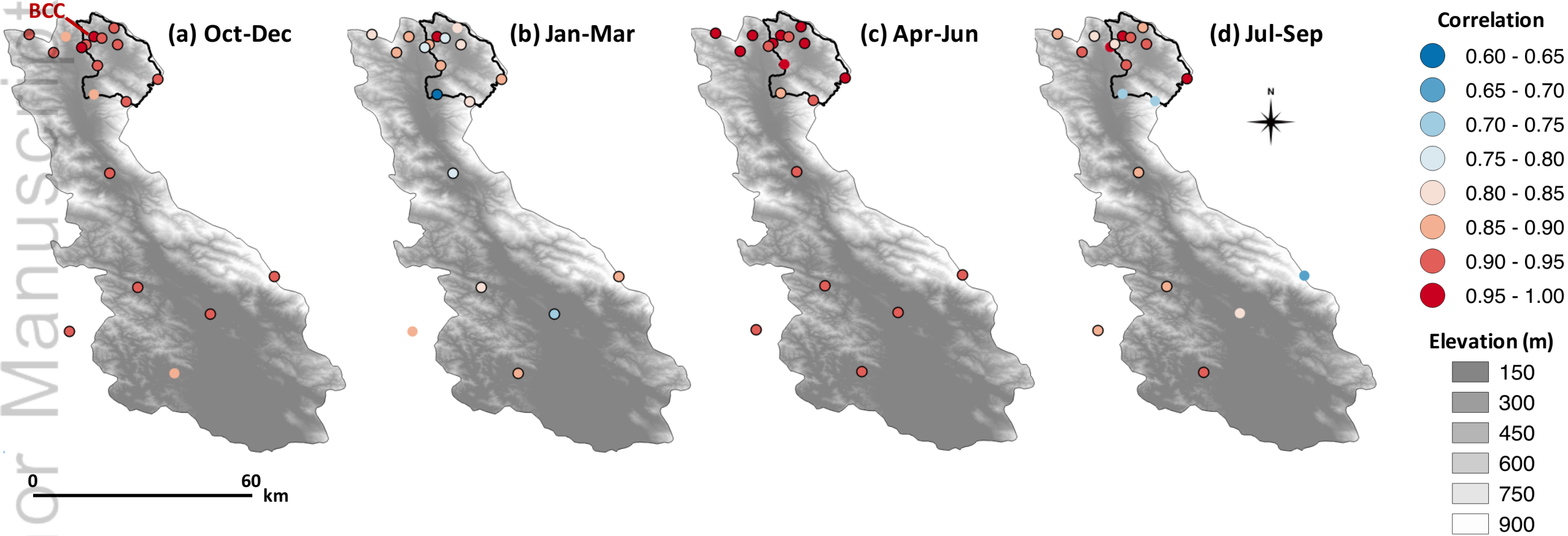

Figure 8. Pearson's correlation maps of 2-minute soil moisture VWC_n with BCC site at 10-cm depth for (a) autumn (Oct–Dec), (b) winter (Jan–Mar), (c) spring (Apr–Jun), and (d) summer (Jul–Sep) of WYs 2018-2019. The thick black contours demarcate the Lake Mendocino Sub-basin. The sites where the correlations are statistically significant at 99% significance level are outlined in black.

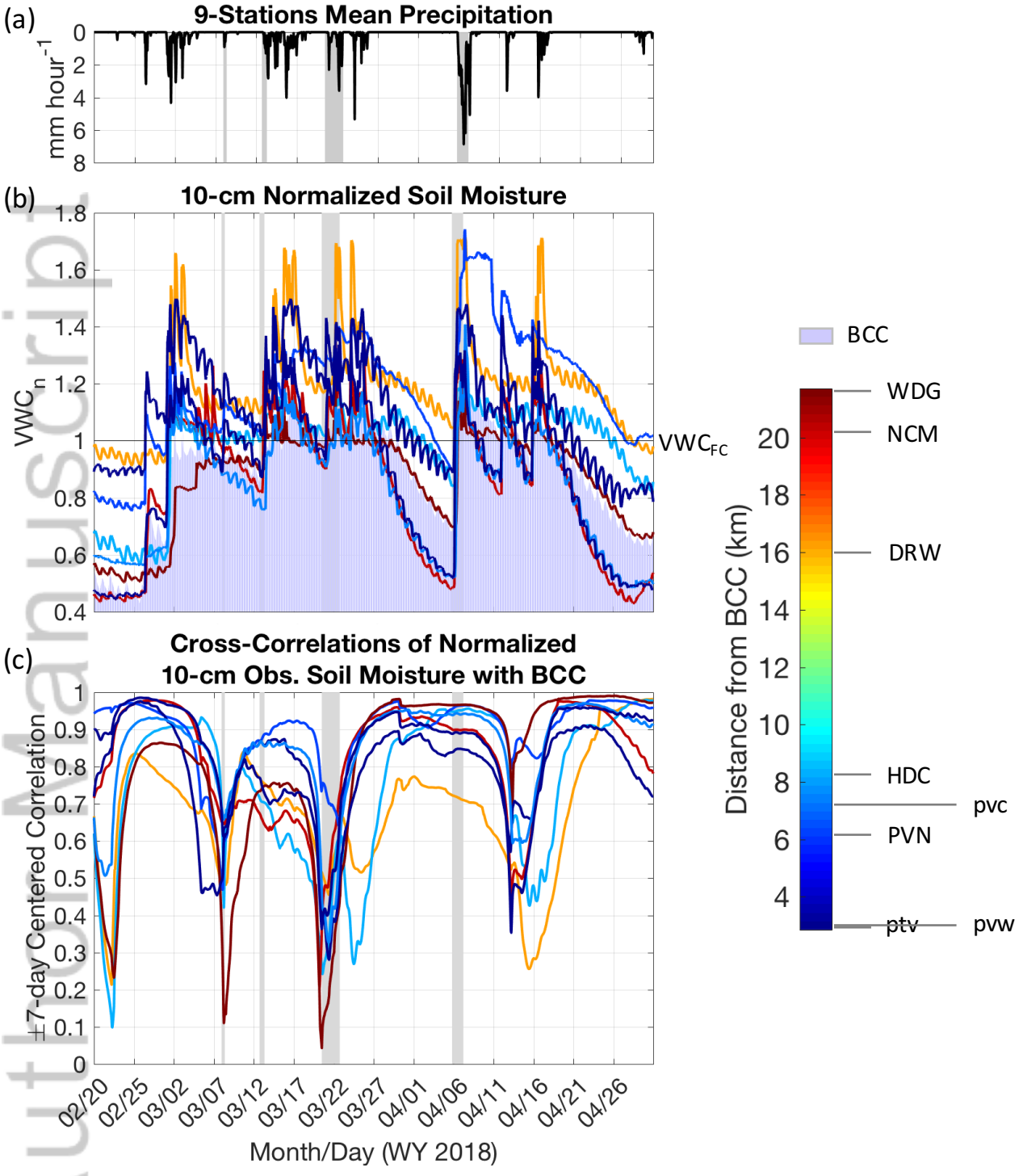

Figure 9. Mid February–April 2018 time series of (a) hourly precipitation, (b) 2-minute soil moisture VWC_n at 10-cm depth, and (c) ±7-day centered cross-correlations of 2-minute soil moisture VWC_n at 10-cm depth with the BCC site. The gray shadings demarcate AR periods. The plot colors on the middle and bottom panel denote site distances from BCC.

A Soil Moisture Monitoring Network to Assess Controls on Runoff Generation During Atmospheric River Events

Edwin Sumargo[1], Hilary McMillan[2], Rachel Weihs[1], Carolyn Ellis[1], Anna M. Wilson[1], and F. Martin Ralph[1]

[1]*Center for Western Weather and Water Extremes, Scripps Institution of Oceanography, University of California San Diego, La Jolla, CA, USA*

[2]*Department of Geography, San Diego State University, San Diego, CA, USA*

Graphical Table of Content

We present a publicly available, high-resolution soil moisture dataset from Russian River Basin in California designed to assess soil moisture controls on runoff generation under atmospheric river conditions. Analyses of the results demonstrate that: (1) Multi-depth sensors are valuable for identifying which depths show differences in evapotranspiration and soil saturation dynamics, (2) Understanding the factors influencing event runoff ratio during a precipitation event enables us to design evaluation techniques and indicates soil moisture processes that distributed hydrologic models should replicate.

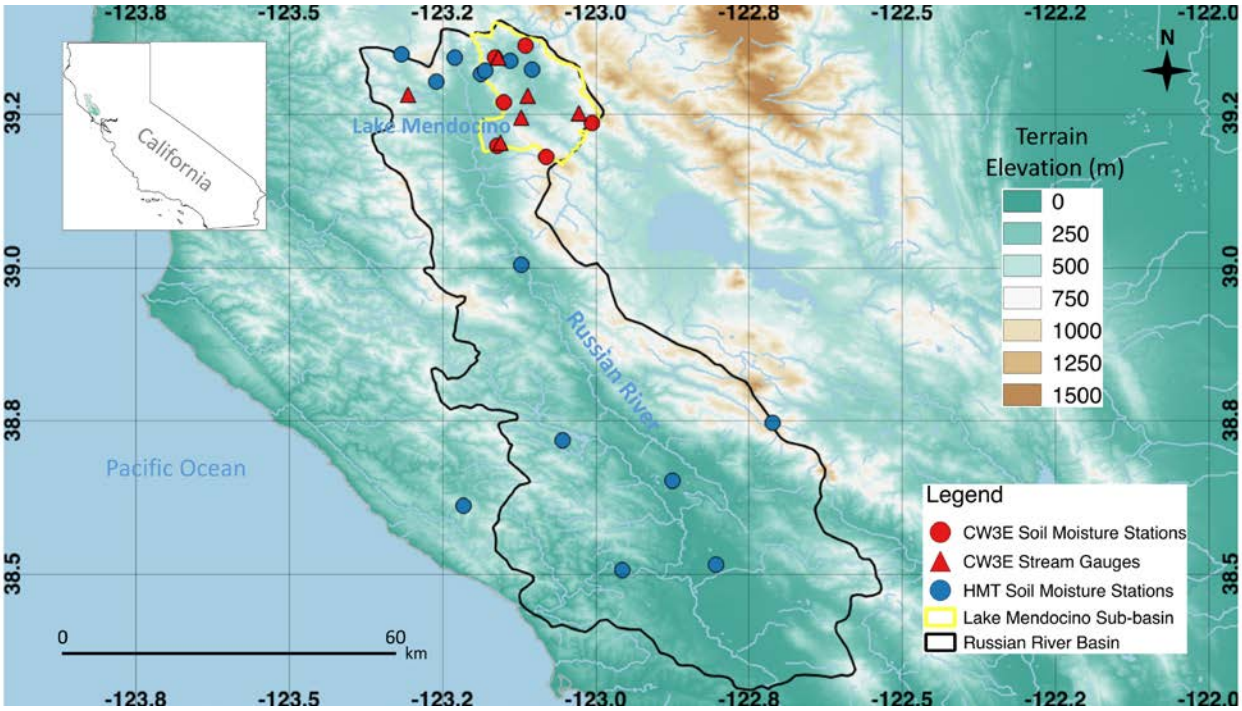

Figure 1. Terrain base map showing the locations of 19 CW3E and HMT soil moisture stations and 6 CW3E stream gauges in Russian River Basin and Lake Mendocino Sub-basin in California.